Spectral FPGA triggers for detection of very inclined showers in the surface detectors of the Pierre Auger Observatory

Zbigniew Szadkowski*

*University of Łódź, Department of Physics and Applied Informatics, 90-236 Łódź, Pomorska 149/151, Poland
†Observatorio Pierre Auger, Av. San Martín Norte 304 (5613) Malargüe, Prov. Mendoza, Argentina

***Abstract*. A new spectral trigger based on the 16-point Discrete Cosine Transform (DCT) algorithm and implemented into a FPGA is described. The DCT trigger allows recognition of FADC traces with a very short rise time and fast exponential attenuation related to a narrow, flat muon component of very inclined Extensive Air Showers generated by hadrons and starting their development early in the atmosphere. The DCT, based on only real coefficients in the frequency domain, provides much more sensitive trigger conditions and a simpler interpretation in comparison to a Discrete Fourier Transform (DFT) that is based on complex coefficients. The ratio of the DCT coefficients to the 1^{st} harmonics depends only on the shape of signals, not on their amplitudes.**

***Keywords*: DCT, FFT, FPGA.**

I. INTRODUCTION

The surface detector of the Pierre Auger Observatory is a 1600 water Cherenkov tank array on a triangular 1.5 km grid. Ultra-relativistic particles in air showers passing through the water generate the Cherenkov light, which is detected by three 9-inch photo-multiplier tubes (PMTs) [1].

Two main triggers are implemented at the 1^{st} level [2]. The first is a single-bin trigger generated as 3-fold coincidence of the 3 PMTs at a threshold equivalent to 1.75 Vertical Equivalent Muon (I_{VEM} - the reference unit for the calibration of FADC traces signals [3] corresponding to ca. 50 ADC-counts). This trigger is used mainly to detect fast signals, which correspond also to the muonic component generated by horizontal showers.

The 2^{nd} trigger is the Time over Threshold (ToT) trigger that requires at least 13 time bins above a threshold of 0.2 I_{VEM}. A pre-trigger ("fired" time bin) is generated if in a sliding time window of 120*25 ns length a coincidence of any two channels appears. It is designed mainly for selecting small but spread-in-time signals, typical for high energy distant EAS or for low energy showers, while ignoring the single muon background.

Cherenkov light generated by very inclined showers crossing the Auger tank can reach the PMT directly without reflections on Tyvec® liners (Fig. 1). Especially for "old" showers the muonic front is very flat [4]. This together corresponds to very short direct light pulse falling on the PMT and in consequence very short rise time of the PMT response. For vertical or weakly inclined showers, where the geometry does not allow reaching the Cherenkov light directly on the PMT, the light pulse is collected from many reflections on the tank walls. Additionally, the shower developed for not so high slant depth are relatively thick. These give a signal from a PMT as spread in time and relatively slow increasing. Hadron induced showers with dominant muon component give an early peak with a typical rise time mostly from 1 to 2 time bins (by 40 MHz sampling) and decay time of the order of 80 ns [5]. The estimation of the rise time on the base with a 25 ns grid is rather rough. Higher time resolution is strongly recommended. The expected shape of FADC traces suggests to use a spectral trigger, instead of a pure threshold analysis in order to recognize the shape of the FADC traces characteristic for the traces of very inclined showers. The monitoring of the shape would include both the analysis of the rising edge and the exponentially attenuated tail.

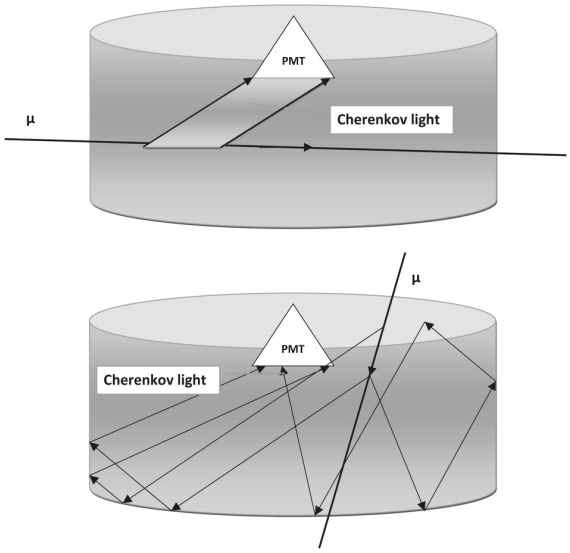

Fig. 1: A geometry of Cherenkov light paths for horizontal and vertical muons crossing the Auger tank.

A very short rise time together with a relatively fast attenuated tail could be a signature of very inclined showers. We observe numerous very inclined showers crossing the full array but which "fire" only few surface detectors (see Figure 2). For that showers much more tanks should have been hit. Muonic front produces PMT signals not high enough to generate 3-fold coincidences,

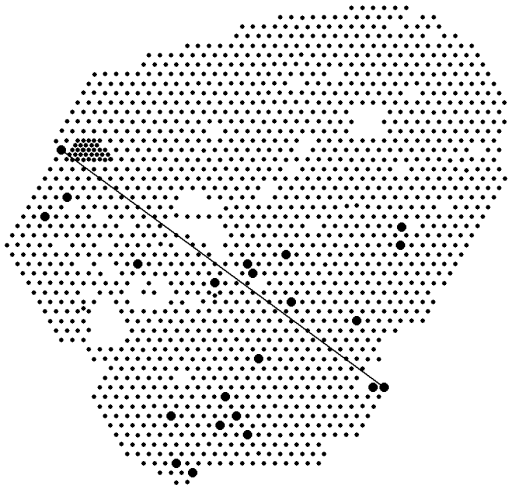

Fig. 2: Position of triggered tanks on the Auger array of event nr 1208896. Muons triggered only few detectors although they should have crossed partially ten or more tanks. A distance between opposite tanks is 54.9 km.

some of signals are below of thresholds. This is a reason of "gaps" in the array of activated tanks.

A next-generation of the Auger Observatory ("Auger North") is currently being designed. It is intended to be located in Colorado, USA, and be larger in size than the Southern Observatory in Mendoza, Argentina. In order to improve the time resolution of measured events and consequently the pointing accuracy of the surface detector, the specification of the surface electronics assumes 100 MHz sampling of the analog signals [6]. For this reason SD electronics for the Auger North requires a new Front-End [7].

The 100 MHz sampling chosen for the Auger North is a compromise between a requirement of improvements (better time resolution) and a hardware limitation (i.e. keeping power consumption on the level appropriate for a solar panel supply, an adjustment of a trigger rate and a size of transmitted data for the bandwidth of the microwave link).

The Auger North design assumes to use a single PMT in each surface detector. The coincidence technique for a noise suppression cannot be used any longer. In order to keep a reasonable trigger rate and not to saturate the communication channel, the trigger threshold has to be significantly increased. But, this yet more reject under-threshold signals. The new spectral approach allows a recognition of a shape of signals independently of their amplitudes. However, this requires a new hardware trigger to assure registered events also for off-line analysis.

II. Spectral triggers

A spectral trigger based on Discrete Fourier Transform (DFT) (Radix-2 FFT) [8] has been already tested in the 3^{rd} generation of the Front End Board (FEB) based on Cyclone™ Altera® chip [9]. It was tested for several weeks in the test tank simultaneously with the standard Threshold and ToT triggers. However, tuning of boundaries for DFT coefficients looked not unequivocally converging procedure relating to the trigger rate. Automatically tuned boundaries allowed also a registration of events with rather not expected shape. This was a motivation to look for an other approach with simpler interpretation of parameters. A comparison of DFT and DCT structures suggested simpler interpretation of the DCT coefficients more suitable for triggers (compare graphs on Figure 3).

The DFT for a real signal x_n : $\bar{X}_{\frac{N}{2}+k} = \bar{X}^*_{\frac{N}{2}-k}$ and $\frac{N}{2}^{th}$ spectral line of $\bar{X}_k$, k = 0,1,...,N-1 is lying on a symmetry axis: the real part is symmetric, the imaginary part is asymmetric. The useful information is contained only in 1^{st} $\frac{N}{2}+1$ spectral lines for k = 0,1,...,N/2 corresponding to frequencies $f_k = k \cdot f_0 = k\frac{1}{N\Delta t}$, changing from zero to $\frac{f_{smpl}}{2}$ with $\frac{f_{smpl}}{N}$ grid.

The new spectral trigger based on the DCT can be implemented only in the new FPGA. Previous generations of the FPGA did not contain enough resources.

The new DCT trigger allows:

- good trigger efficiency on very inclined showers,
- an opportunity to built more sophisticated triggers in one Auger North design where each tank will be equipped with only one PMT. Noise reduction by the coincidences technique is no longer possible.

There are several variants of the DCT with slightly modified definitions. The most commonly used form of the transform (DCT-II) defined as follows:

$$\bar{X}_k = \alpha_k \sum_{n=0}^{N-1} x_n cos\left(\frac{\pi}{N}\left(n+\frac{1}{2}\right)k\right)$$

The selected DCT-II variant is a Fourier-related transform similar to the DFT, but using only real numbers. DCTs are equivalent to DFTs of roughly twice the length, operating on real data with even symmetry (since the Fourier transform of a real and even function is real and even). The DCT for real signal x_n gives independent spectral coefficients for k = 0,1,...,N-1, changing f_k also from zero to $\frac{f_{smpl}}{2}$, but with $\frac{f_{smpl}}{2N}$ grid. DCT vs. DFT gives twice better resolution.

The DCT algorithm presented in the paper has a significant advantage in comparison to the FFT one. The structure of DCT coefficients are much simpler for interpretation and for a trigger implementation than the structure of the FFT real and imaginary coefficients (compare 4^{th} of the FFT data vs. 2^{nd} row for the DCT coefficients in Figure 3). For the exponentially attenuated signals from the PMTs higher DCT coefficients (scaled to the 1^{st} harmonics) are almost negligible, while both real and imaginary parts of the FFT (scaled to the module of the 1^{st} harmonics) give relatively significant contributions and are not relevant for triggering. When a peak appears in the pure attenuated signal (last column in Figure 3) the structure of the DCT dramatically changes and trigger condition immediately expires, while modules of FFT components almost do not change.

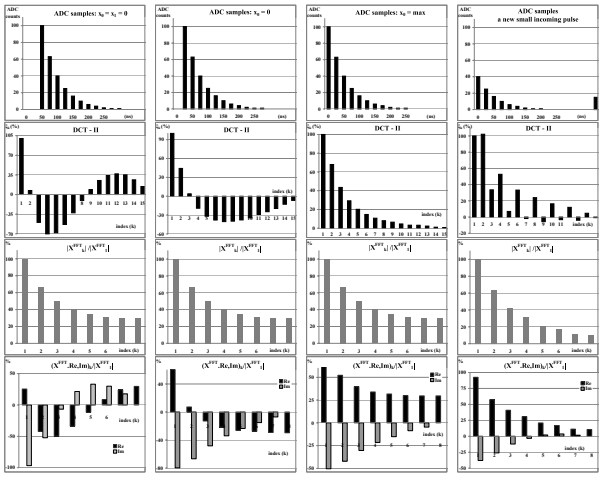

Fig. 3: A propagation of the pulse (1^{st} row) through the shift register, DCT-II (2^{nd} row), $\|DFT\|$ (3^{rd} row) and real (Re), imaginary parts (Im) (4^{th} row), respectively. Shape A corresponds to the the pulse, when two time bins are on the pedestal level, shape B, when only the one time bin is still on the pedestal level, while shape C shows the pulse fully fulfilled the range of investigating shift registers. For a signal shape C related to the exponential attenuation, the contribution of higher DCT coefficients is small and suitable for a trigger. When a peak appears in the declining signal (shape D), the DCT coefficients immediately excesses assumed relatively narrow acceptance range for triggers. The DFT coefficients (Re and Im in 4^{th} row) have similar structure as the DCT, however for the pure exponentially declining signal the higher real DFT harmonics have relatively high values and they are not suitable for triggering. $\|DFT\|$ are clearly insensitive on discussed conditions.

The structure of FFT harmonics for the last graph in Figure 3 would be more suitable for a trigger (almost negligible imaginary part for higher harmonics and also relatively low real harmonics), however it corresponds just to situation, when the pure attenuated signal is distorted by some peak on the tail and a trigger condition has been violated.

The plot in the 4^{th} row and 3^{rd} column on Figure 3 shows a contribution of the DFT vs. the absolute value of the 1^{st} harmonic. For a exponential attenuated input signal (with the attenuation factor = β) the contribution of both real and imaginary coefficients decreases monotonically with a significant value for all real coefficients. From the DFT definition and for boundary factors β = (0.28, 0.42) (taken the Auger data) and for k = N/2 (as the lowest in a monotonically decreasing chain), we obtain for N = 16: ξ = 24% and 28% respectively. These values are too large to be use for triggering. Even an extension of the DFT size does not help very much. For N = 32: we get still large values: ξ = 17% and 23%.

Almost vanishing higher DCT factors provide much natural trigger conditions. 32-point FFT (roughly equivalent to 16-point DCT) does not offer better stability.

The trigger described in [8] is based on a 16-point FFT algorithm and is clocked with 40 MHz. The "length" of the analyzing sliding window equals to 400 ns, which is sufficient for an analysis of the muonic bump, especially for the "old" showers.

For the new 100 MHz sampling, 16-point samples would correspond to a 150 ns sliding window only. An analysis of the Auger database (collected for 40 MHz sampling) showed that a "length" of FADC traces corresponding to 200-250 ns is desirable.

The analysis of the attenuation part of the Auger FADC traces gives an attenuation factor roughly independent of time. FADC traces of almost very inclined events are characterized by a dramatic jump from the pedestal level up to maximal value due to their origin related to the geometrical configuration of PMTs in the tank (Figure 1).

The 100 MHz sampling however, should be already sensitive on a signal shape especially in the range of the rising edge of the analog signal, which corresponds to the beginning of the muonic shower. This region contains crucial information and should be sampled with full resolution. The tale of the signal, much longer than its front, contains less important information and can be sampled with a bigger grid. For 8 first samples in a 10 ns grid and next 8 samples in a 20 ns grid, the "length" of an analyzing sliding window is 230 ns and seems to be sufficient for our analysis.

The analog section of the FEB has been designed to have a pedestal of ca. 10% of the full FADC range in order to investigate the undershoots. It is easy to proof, that for $k \geq 1$ the DCT coefficients $\bar{X}_k$ are independent of the pedestal.

The DCT coefficients normalized to the 1^{st} harmonics $\xi_k = \frac{\bar{X}_k}{\bar{X}_1}$ are also invariant on the scaling of a signal amplitude. As seen from Figure 3, if ADC samples propagating in the shift registers, which drive the DCT routine, match the pattern of exponential attenuation, the contribution of higher ξ_k significantly drops down. The level of ξ_k contributions can be used to for a preliminary spectral trigger. If in the propagating signal a sample, significantly different from an expecting shape, appears in the input shift register, ξ_k dramatically change and stop fulfilling a trigger condition.

Propagation of pulses for three different rise times and two attenuation factors (0.28, 0.42) is shown on Figure 4. These factors have been estimated upon the real events registered on the field. We expect that the pulses from the very inclined and horizontal showers will be attenuated with a factor between estimated minimal and maximal limits. Thus the corresponding spectral coefficients ξ_k are in very narrow ranges suitable for triggering.

Figure 5 show the ranges of the ξ_k coefficients allowing a generation of the sub-triggers. If for the investigated shape of the pulse and for the index k, the spectral coefficient ξ_k is inside the range showing in the corresponding graphs $B', C', D'_{1,2,3}$, the sub-trigger$_k$ is

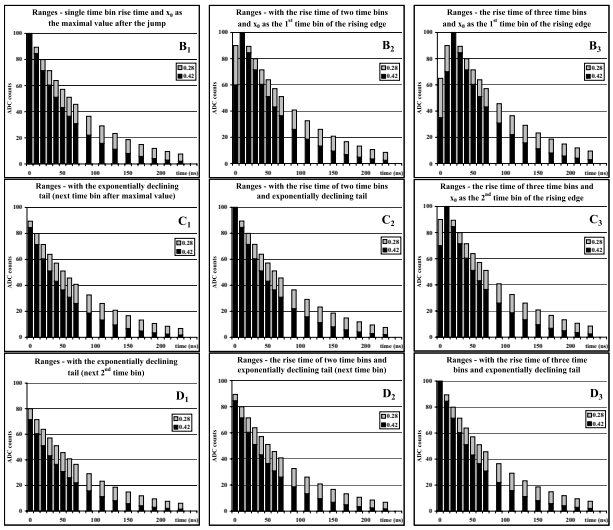

Fig. 4: Propagation of pulses with the single (1^{st} column), two (2^{nd} column) and three (3^{rd} column) time bins of the rising edge for four consecutive time bins. Two shapes of signals are presented for boundary attenuation factors: β = 0.28 and 0.42 respectively. Shapes B_1, C_1, D_1, C_2, D_2 and D_3 correspond to pure exponentially attenuated signals.

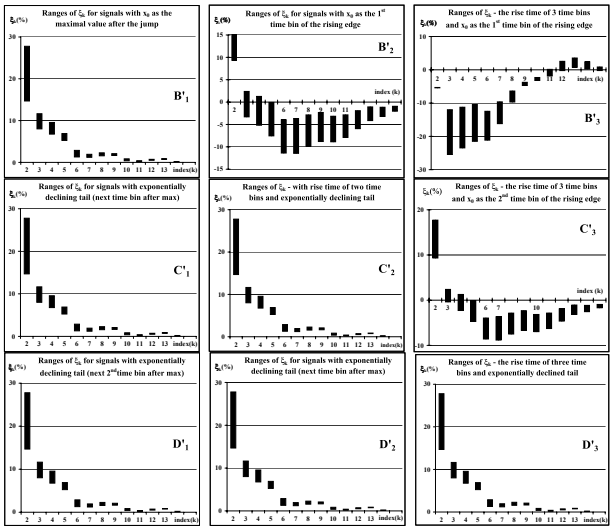

Fig. 5: Ranges of allowed ξ_k coefficients corresponding to signals from Figure 4. As expected, the ξ_k set for exponentially declining tails (B_1, C_1, D_1, C_2, D_2 and D_3 from Figure 4) are very similar (compare graphs: B'_1, C'_1, D'_1, C'_2, D'_2 and D'_3). By taking into considerations of the noise the sets of ξ_k for these cases are established as the same. The noise constrains also an adequate expansion of ξ_k ranges.

generated. For exponentially declining tails the ξ_k set are very similar.

However, the analysis of the pure attenuated signals is the only part of trigger process. We are going to select pulses with a fixed rise time and the exponential attenuation tail with a dedicated circuit ("engine") recognizing required shape. If the "engine" is fixed for a recognition of the shape with i.e. two time bins (graphs B_3, C_3, D_3), the trigger circuit is waiting for the set of ξ_k corresponding to the graph B'_3. We do not require all ξ_k coefficients have to be inside the acceptance range. We allow 2 or 3 coefficients could be outside the acceptance lane. This mitigation should improve the trigger condition. A requirement when all ξ_k have to be inside the acceptance range seems to be too strong and could bias significantly a trigger rate.

If a number of ξ_k are above the "occupancy" threshold (the shape B'_3 has been recognized), the multiplexer changes the set of the expected limits for the ξ_k and in the next clock cycle the circuit is waiting for the set of ξ_k corresponding to the graph C'_3. If this shape is also recognized, the circuit in the next two clock cycles is waiting for the pure attenuated signal related to the graphs D'_3. A similar analysis is performed for the shapes related to graphs B_1, C_1, D_1 and B_2, C_2, D_2.

An approach based on the exponentially declining signal (shape A) only may give too high trigger rate due to single muons. However, this trigger verifies a purity of the exponential shape of signal. An internal FPGA routine calculating the DCT coefficients is derived from the well-known algorithm of Arai-Agui-Nakajima [10], however significantly optimized for the FPGA [11].

III. SUMMARY

Spectral triggers are being optimized in the Auger South test detectors with the configuration of 3 "engines" and 3-fold coincidences working for the single selected shape B_k, C_k, D_k (Figure 5). According to estimations, the configuration with 3 "engines" does not support all ξ_k sub-triggers due to limited amount of DSP blocks. However, the neglected coefficients are not specially relevant. For the Auger North for the single PMT, 3 "engines" will be implemented to investigate and to detect 3 different shapes of FADC traces corresponding to different rise time of the rising edge [12].

Furthermore, the implementation of the algorithm presented above may be applied in on-line video signal processing, where Discrete Cosine Transform is widely used.

REFERENCES

[1] J. Abraham et al., [Pierre Auger Collaboration], Nucl. Instr. Meth. **A523**, (2004) 50-59.
[2] D. Allard, et. al, *in Proc. 29th ICRC*, Pune, 2005.
[3] M. Aglietta, et. al, *in Proc. 29th ICRC*, Pune, 2005.
[4] L. Nellen *in Proc. 29th ICRC*, Pune, 2005.
[5] M. Aglietta, et. al, *in Proc. 29th ICRC*, Pune, 2005.
[6] http://www.auger.org/admin/index.html, Auger North Report,
[7] Z. Szadkowski, *Proc. 31st ICRC*, Łódź, Poland, 2009.
[8] Z. Szadkowski, *Nucl. Instr. Meth.*, **A560**, pp. 309-316, 2006.
[9] Z. Szadkowski, K-H. Becker, K-H. Kampert, *Nucl. Instr. Meth.*, **A545**, pp. 793-802, 2005.
[10] Y. Arai, T. Agui, M. Nakajima. *Trans. IEICE*, **E-71**, no. 11, pp. 1095-1097, 1988
[11] Z. Szadkowski, NSS & MIC, IEEE, Dresden 2008.
[12] Z. Szadkowski,, *Nucl. Instr. Meth.*, 2009, in print.